Biocatalysis and Agricultural Biotechnology 20 (2019) 101251

Contents lists available at ScienceDirect

Biocatalysis and Agricultural Biotechnology

journal homepage: www.elsevier.com/locate/bab

Biogenic synthesis of ferric oxide nanoparticles using the leaf extract of *Peltophorum pterocarpum* and their catalytic dye degradation potential

Sanjana Anchan[a], Shraddha Pai[a], H Sridevi[a], Thivaharan Varadavenkatesan[b], Ramesh Vinayagam[c], Raja Selvaraj[c,*]

[a] Department of Civil Engineering, Manipal Institute of Technology (MIT), Manipal Academy of Higher Education (MAHE), Manipal, Karnataka, 576104, India
[b] Department of Biotechnology, Manipal Institute of Technology (MIT), Manipal Academy of Higher Education (MAHE), Manipal, Karnataka, 576104, India
[c] Department of Chemical Engineering, Manipal Institute of Technology (MIT), Manipal Academy of Higher Education (MAHE), Manipal, Karnataka, 576104, India

ARTICLE INFO

Keywords:
Peltophorum pterocarpum
Green synthesis
Fe_2O_3 nanoparticles
Fenton-like catalysis
Methylene blue dye
$NaBH_4$ reduction

ABSTRACT

Plant-mediated green synthesis of nanoparticles is an eco-friendly and cheap method since it makes use of phyto-compounds present in various plant parts as reducing and stabilizing agents. Herein, magnetic, ferric oxide nanoparticles (FONPs) were prepared by utilizing the leaf extract of *Peltophorum pterocarpum* for the first time. Rod-like FONPs with agglomerations were witnessed in FE-SEM images. Sharp peaks for elemental oxygen and iron were witnessed in EDS spectrum. XRD spectrum ascertained the crystallinity of the FONPs and showed both γ and α–Fe_2O_3 phases. The average crystallite size was 16.99 nm. A large specific surface area (66.44 m^2/g) was found in BET analysis and the FONPs were mesoporous (pore diameter = 7.92 nm). TGA results showed a 20% weight loss during heating up to 800 °C. FTIR spectrum showed significant bands for various phyto-compounds and Fe–O. The Fenton-like catalytic efficiency of FONPs was studied for the methylene blue dye degradation during which 90% removal was noticed within 220min. The experimental results were satisfactorily fitted into a second-order model with a degradation constant of 0.0987 L/mg min. Also, the catalytic activity of the FONPs was assessed for the removal of MB dye with the reducing agent $NaBH_4$. A remarkable dye degradation (92%) was attained within 27min, and the results were best suited for a first-order model with a kinetic degradation constant of 0.0856min^{-1}. Therefore, the green-synthesized FONPs obtained here could be used in the degradation of dyes as nanocatalysts for the remediation of wastewater.

1. Introduction

The field of nanotechnology is an upcoming research area which has multifaceted applications (Thivaharan et al., 2018). This field has grown by leaps and bounds over the past two decades owing to the unique features of the nanoparticles such as small size, high surface area, catalytic activity, specific optical property, sensing capacity, biocompatibility, antibacterial activity, antioxidant activity, and adsorptive ability etc (Amstad et al., 2011; Hussain et al., 2016; Ju-Nam and Lead, 2008; Raghunath and Perumal, 2017; Schröfel et al., 2014). Amidst various nanoparticles, ferric oxide nanoparticles (FONPs) are one of the most important types of metal oxide nanoparticles because of its salient characteristics like magnetic property, biocompatibility and high surface to volume ratio (Mishra and Chun, 2015). Therefore, they are used in many environmental applications such as catalysis, adsorption of many dyes, heavy metals, and antibiotics from wastewater (Carvalho and Carvalho, 2017)(García et al., 2019).

There are many conventional methods available to synthesize FONPs, like co-precipitation, micro-emulsion, sol-gel, solvothermal, thermal decomposition and chemical methods. Nevertheless, these processes utilize high-priced and toxic chemicals and employ energy-intensive processes. To overcome the drawbacks as mentioned above of conventional synthesis processes, nowadays, an environmentally benign method which makes use of plant extracts, popularly known as "plant-mediated green synthesis" is becoming attractive owing to the less cost, eco-friendliness, and rapidness (Kharissova et al., 2013). The increase in the number of published articles using plant extracts to synthesize nanoparticles witnesses the significance of this method (Peralta-Videa et al., 2016).

The plant extracts contain various phyto-compounds which act as both capping and reducing agent to form nanoparticles (Sathiyavimal et al., 2018). Moreover, the standard reduction potential of these phyto-compounds is around 0.534 V whereas it is −0.44 V for metallic iron and therefore the reduction process is spontaneous (Groiss et al., 2017).

* Corresponding author.
E-mail address: raja.s@manipal.edu (R. Selvaraj).

https://doi.org/10.1016/j.bcab.2019.101251
Received 10 June 2019; Received in revised form 11 July 2019; Accepted 15 July 2019
Available online 16 July 2019
1878-8181/

Apart from the reduction, the phyto-compounds surround the nanoparticles thereby providing stability and unique morphology(Makarov et al., 2014)(Varadavenkatesan et al., 2019).

According to a brief literature review, there are only a few articles which report the synthesis of FONPs by plant sources. Few examples include, the leaf extract of *Camellia sinensis* (Ahmmad et al., 2013), *Eucalyptus Globulus* (Balamurugan et al., 2014), *Aloe vera* (Mukherjee et al., 2016), *Sageretia thea* (Khalil et al., 2017), *Ailanthus excels* (Asoufi et al., 2018), *Rhus punjabensis* (Naz et al., 2019), root extract of *Arisaema amurense* (Narayanan and Sung, 2016) and fruit extract of *Cynometra ramiflora* (Bishnoi et al., 2018) which were used recently to synthesize FONPs. However, there is no report on the preparation of FONPs utilizing the leaf extract of *Peltophorum pterocarpum*. This tree is also known as copper pod tree, and the reduction capacity of the leaf extract has previously been explored by our research team for the preparation of ZnO nanoparticles (Pai et al., 2019). Hence, the green synthesis of FONPs by a sustainable material, the leaf extract of *P.pterocarpum* is considered here as a novel area of research.

There are many dyes used in textile, dyeing, paper and tannery industries which generate a lot of dye-laden wastewater effluents that pose an environmental threat (Fathima et al., 2018) (Saratale et al., 2018). Removal of these dyes from the wastewater is one of the challenges in the environmental field (Nandhini et al., 2019). Biological methods and other conventional methods such as adsorption, electrodialysis, ozonation, photochemical methods are either costly or low-efficient. However, an advanced oxidation process which is popularly known as the Fenton-like process is a powerful method for the remediation of dye-laden wastewater (Xue et al., 2009). This process makes use of iron oxide or zero-valent iron nanoparticles as the source for the generation of hydroxyl radicals when reacts with hydrogen peroxide whereas the conventional Fenton process utilizes the dissolved ferrous ions (from ferrous sulfate) as the source (Wang et al., 2016). The significant advantages of the Fenton-like process are mild operating conditions (non-acidic/circumneutral pH) (Xue et al., 2009) and the avoidance of sludge formation at the end of the treatment process (Zha et al., 2014).

Therefore, in the present study, the objectives are to (1) synthesize and characterize the magnetic FONPs by making use of the water extract of *P.pterocarpum* leaves; (2) examine the Fenton-like catalytic efficiency and (3) study the catalytic potential of the synthesized FONPs to degrade methylene blue (MB) dye, a model pollutant, with the reductant $NaBH_4$.

2. Materials and methods

2.1. Materials

Ferrous sulfate heptahydrate ($FeSO_4.7H_2O$), NaOH, $NaBH_4$ and MB dye were obtained from Merck, India.

2.2. Peltophorum pterocarpum leaf extract preparation

The leaves were collected in the month of August, in our university premises. The leaf extract of *P.pterocarpum* was prepared following our earlier report (Pai et al., 2019). The leaf extract was named as “Copper Pod Leaf Extract” (CPLE) and kept at 4 °C for future usage.

2.3. Synthesis of FONPs

0.1 M $FeSO_4.7H_2O$ solution and CPLE at 1:1 (v/v) were mixed in a flask, and 2M NaOH was added intermittently to this mixture. The contents turned to black colored solution upon boiling for 60 min in an electrical heater which suggested the formation of ferric oxide nanoparticles (CP–FONPs). The formed nanoparticles were parted from the solution by a magnet and washed periodically with distilled water. Later, they were oven-dried at 100 °C, for 8 h and kept in a container for subsequent usage.

2.4. Fenton-like catalytic activity of CP–FONPs for the degradation of MB dye

Fenton-like catalytic experiments were conducted at room temperature in a rotary shaker. The experimental procedure was similar to the one, reported elsewhere(Shahwan et al., 2011), with few modifications. Briefly, 45 mL of 25 ppm MB dye, 5 mL of 10% H_2O_2 and 50 mg of CP–FONPs were taken in a conical flask and kept in the rotary shaker at 150 rpm. At regular time intervals, samples were collected from the reaction mixture using a magnet. UV–Visible spectrophotometer (UV-1700, SHIMADZU) was employed to record the absorbance spectrum. The concentration of the dye was determined using a standard plot which was recorded at 665 nm (λ_{max}). The kinetic data of MB dye degradation were fitted to the first and second-order rate equations (Shahwan et al., 2011). The design equations for both are given by (Eqn. (1) & (2)),

$$ln\left[\frac{C_t - C_e}{C_o - C_e}\right] = -K_1 t \quad (1)$$

$$\left[\frac{1}{C_t - C_e}\right] - \left[\frac{1}{C_o - C_e}\right] = K_2 t \quad (2)$$

where, C_o, C_t, and C_e are the concentrations of MB dye at the initial stage, at any time ‘t' and equilibrium respectively. K_1 and K_2 denote the first and second order degradation rate constants respectively.

2.5. Degradation of MB dye in the presence of CP–FONPs and $NaBH_4$

The catalytic degradation of MB dye in the presence of CP–FONPs, and $NaBH_4$ was carried out according to the procedure given in the literature (Cheera et al., 2016) with slight modifications. The procedure involved was as follows: 3 mL of MB dye (20 ppm) was taken in a clean quartz cuvette and freshly prepared 300 µL $NaBH_4$ (100 mM) was added. To this reaction mixture, 15 mg of CP–FONPs was added, and the variations in the absorbance spectra were monitored continuously. The obtained kinetic data were considered for fitting into first and second order models (Eqn. (1) & (2)).

2.6. Characterization of CP–FONPs

The purified CP–FONPs were characterized by various techniques. The surface morphology and individual elements present in the sample were analyzed using Field Emission Scanning Electron Microscope (FE-SEM), Carl Zeiss (ZEISS, Sigma) and EDS respectively. X-Ray diffractometer (Rigaku Miniflex 600) was used to determine the crystallinity of the CP–FONPs. The specific surface area (SSA) and pore structure were determined by BET instrument (Smart Instruments, Mumbai). TGA data were obtained from TGA55 (0550–0543) instrument (27–800 °C; N_2 atmosphere; 10 °C/min heating rate). The involvement of specific chemical groups was checked from the spectrum obtained from FTIR Spectrophotometer (SHIMADZU, 8400S).

3. Results and discussions

3.1. Synthesis of CP–FONPs and UV–vis studies

The formation process of ferric oxide nanoparticles from the copper pod leaves has been depicted in Fig. 1. Herein, a black colored solution (E) was formed when the brown CPLE (C) was added to 0.1M $FeSO_4$ solution (D) and 2M NaOH while heating for 60 min in an electric heater which indicated the formation of magnetic CP–FONPs (Kumar et al., 2016). This result is concordance with our earlier study for FONPs synthesized using *Cynometra ramiflora* fruit extract(Bishnoi

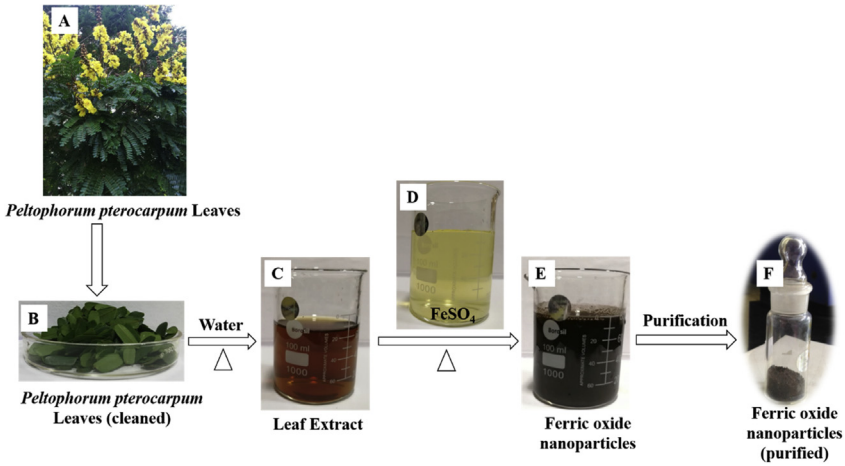

Fig. 1. (A). *Peltophorum pterocarpum* leaves, (B).Cleaned *Peltophorum pterocarpum* (C). Leaf extract, (D). $FeSO_4$ solution, (E). CP–FONPs, and (F) purified CP–FONPs.

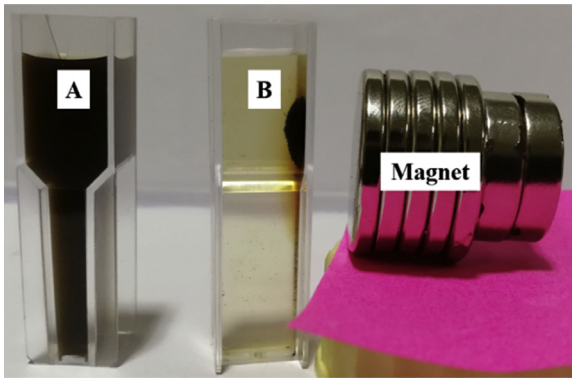

Fig. 2. The magnetic attraction of CP–FONPs (A. CP–FONPs in solution state; B. Magnetic attraction of CP–FONPs towards a magnet).

et al., 2018). The change in coloration is owing to the interaction between the phytochemicals and ferrous ions, and thus spontaneous reduction occurs (Weng et al., 2013). The resulting solution was allowed to settle, and the CP–FONPs were parted by a magnet. Periodical washing with distilled water and drying yielded a black colored product (D). The magnetic attraction of CP–FONPs can be visualized in Fig. 2.

The UV–vis spectral image of the leaf extract and CP–FONPs suspension is shown in Fig. 3. A characteristic peak for the polyphenolic compounds at 273 nm can be visualized from the spectrum of the leaf extract whereas no specific peak was observed for CP–FONPs. This endorses the reduction process between the phyto-compounds of CPLE

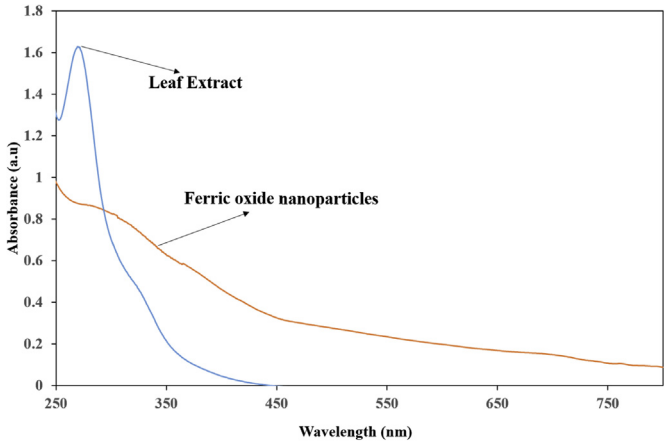

Fig. 3. UV–vis spectrum of leaf extract and CP–FONPs suspension.

and $FeSO_4$ (Groiss et al., 2017). The continuous absorption band of CP–FONPs corroborated the formation of FONPs. This result exactly matches with the UV–vis spectra of the iron-oxide nanoparticles prepared using the *Cynara cardunculus* leaf extract (Ruíz-Baltazar et al., 2019) and seaweed extract (Yew et al., 2016). The prominent absorption spectrum in the visible region has been reported for green-synthesized iron oxide nanoparticles by many researchers (Dash et al., 2019; Hoag et al., 2009; Njagi et al., 2011; Sirdeshpande et al., 2018).

3.2. SEM & EDS

The SEM image (Fig. 4) at two different magnifications displays the morphology of the CP–FONPs as irregular rod-like structures. A similar kind of rod-like morphology of FONPs was reported in the literature (Zhang et al., 2012). It is mentioned that the irregular shape of the nanoparticles is common in powdery and porous materials which ascertain relatively rough surfaces (Maji et al., 2012).

A few agglomerations were noticed in the SEM image which might be due to the interactions between the biomolecules and FONPs as mentioned in many green-synthesized iron nanoparticles (Groiss et al., 2017; Huang et al., 2015; Weng et al., 2013) (Aksu Demirezen, Yıldız, Yılmaz, et al., 2019) (Farshchi et al., 2018). Very recently, an article has reported iron oxide nanoparticles utilizing *Ruellia tuberosa* leaf extract with agglomerations (Vasantharaj et al., 2019a). The results are in agreement with another published article where it is mentioned that the agglomeration may be due to the stearic effect ascribed to the interaction of the active sites of nanoparticles and the magnetic nature of the CP–FONPs (Ruíz-Baltazar et al., 2019).

The sharp peaks between 6 and 8 keV in the EDS image (Fig. 5) confirmed the presence of elemental iron (Vasantharaj et al., 2019a). The significant peak at 0.6 keV affirmed the existence of elemental oxygen. These peaks confirm that FONPs were present in the sample. Apart from iron and oxygen, few elements such as sodium, calcium, and silicon were also witnessed in the spectrum which may be caused from the glass slide on which the sample was deposited (Vinayagam et al., 2017) (Vinayagam et al., 2018). The sulfur and sodium peaks must have originated from the $FeSO_4$ precursor and NaOH used in the synthesis process. The atomic percentages obtained from EDS quantification were 56.23% of O, 5.56% of Fe, 30.07% of Na, 1.65% of Si, 6.33% of S and 0.16% of Ca. The atomic compositions of Fe and O obtained in the current study corroborated the existence of FONPs in the sample. Similar proportions were mentioned for the FONPs prepared by utilizing the leaf extract of *Eucalyptus globulus* (Balamurugan et al., 2014) and fruit extract of *Ficus carica* (Aksu Demirezen, Yıldız, Yılmaz, et al., 2019). The high composition of oxygen ascertained the fact that the prepared nanoparticles are in iron oxide form (Aksu Demirezen, Yıldız,

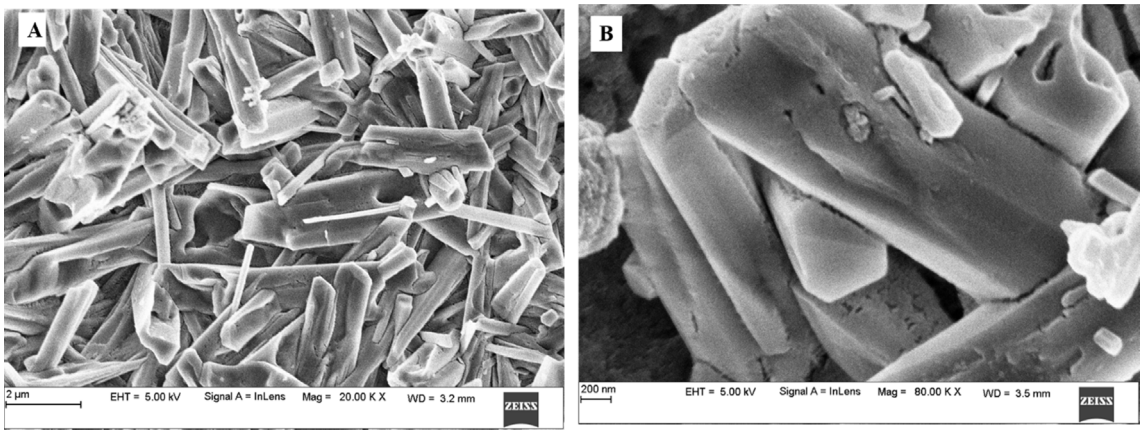

Fig. 4. FE-SEM images of the CP–FONPs (A). 20 kX magnification, (B). 80 kX magnification.

and Demirezen Yılmaz, 2019).

3.3. XRD

The XRD spectrum of the CP–FONPs was depicted in Fig. 6. The image showed three distinct peaks at 2θ (°) = 29.61, 31.73, 34.05 which corresponded to phase planes of (220), (104) and (310) respectively. The peaks at 29.61 and 34.05 and their corresponding planes are in concordance with the standard maghemite (γ-Fe_2O_3) phase [JCPDS Card No. 39–1346](Yu et al., 2010). Furthermore, the peak at 31.73 and its respective plane matches with hematite (α-Fe_2O_3) phase [JCPDS Card No. 33–0664] (Yu et al., 2010). Iron oxide nanoparticles with different phases (γ and α) have been reported already(Sahoo et al., 2010; Yu et al., 2010). The small peak at 21° corresponds to polyphenols of the plant extract (Groiss et al., 2017). Absence of other peaks corroborates the fact that the sample is highly pure Fe_2O_3.

The mean crystallite size of the CP–FONPs was determined as 16.99 nm by using Scherrer's formula (Litvin and Minaev, 2013) which corroborated the nano-range of the FONPs (Table 1). Mean size of 29 nm has been reported for the synthesis of Fe_2O_3 using *Sageretia thea* extracts (Khalil et al., 2017). Equivalently, 33 nm was published for the Fe_2O_3 synthesized using *Camellia sinensis* extract (Ahmmad et al., 2013).

3.4. BET analysis

The SSA and total pore volume of CP–FONPs were 66.44 m^2/g and 0.1315 cm^3/g respectively as given by BET method. The obtained SSA is almost 11 times higher than the commercial Fe_2O_3 (6 m^2/g) (Ahmmad et al., 2013) which indicated the formation of highly porous structure (Guo et al., 2014). The high surface area can be attributed to the small crystal size as obtained in XRD studies. The diameter of the pores was determined as 7.92 nm which substantiated the mesoporous nature of the CP–FONPs. The size of the nanoparticles was determined as 17.23 nm which confirmed the nanosize of the CP–FONPs. The large surface area and mesoscopic structure may render an excellent catalytic property to the CP–FONPs.

3.5. TGA

The TGA curve in Fig. 7 indicated a substantial loss in the weight of CP–FONPs between 27 °C and 800 °C. An initial reduction of 3.81%

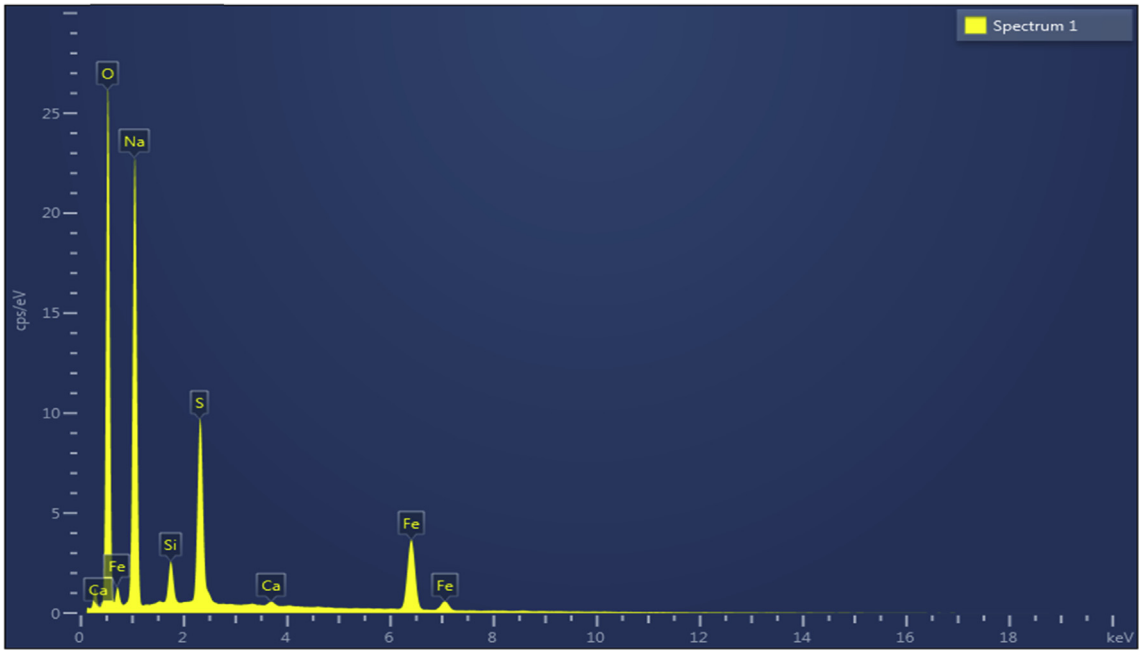

Fig. 5. EDS spectrum of the CP–FONPs.

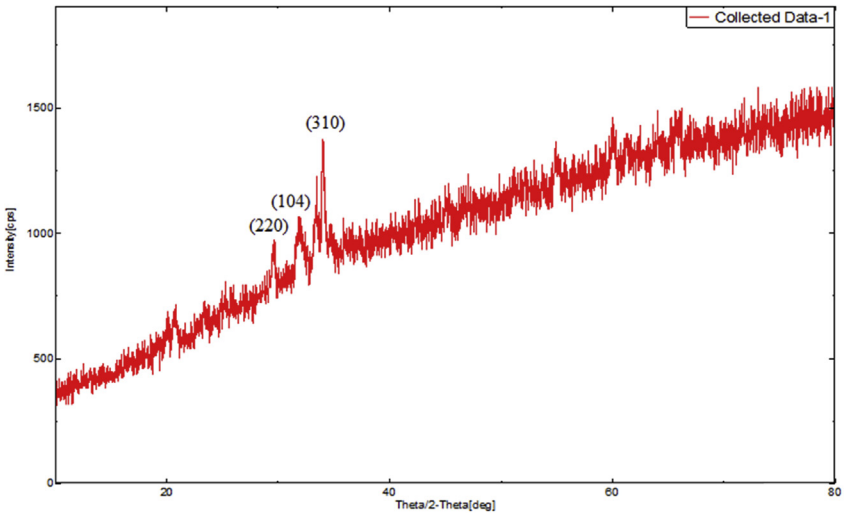

Fig. 6. XRD spectrum of the CP–FONPs.

Table 1
XRD parameters and crystallite parameters of CP–FONPs.

Peak No.	2θ (deg)	Plane (hkl)	Phase	FWHM (deg)	Crystallite size (nm)
1	29.61	220	γ-Fe_2O_3	0.4194	21.05
2	31.73	104	α-Fe2O3	0.7354	12.04
3	34.05	310	γ-Fe_2O_3	0.4932	17.89

(27–100 °C) was observed due to the removal of physisorbed water and other volatile contents present in CP–FONPs (Ahmmad et al., 2013). A weight loss of 4.26% was noticed from 100 to 300 °C which might be due to the decomposition of biomolecules surrounding the CP–FONPs. After that, a steep decrease in weight was observed from 300 to 800 °C (8.22%) which indicated adsorbed oxygen species (Basavegowda et al., 2017). There was a 3.27% weight loss between 700 and 800 °C. Overall, there was a 20% weight loss, and therefore it can be concluded that the weight loss is mainly because of dehydration and decomposition of biomolecules present in the CP–FONPs (Khatami et al., 2019; Sneha and Sundaram, 2015).

3.6. FTIR analysis

The existence of specific functional groups in the CP–FONPs was ascertained using FTIR pattern (Fig. 8) which was measured over the spectral range (4000–400 cm^{-1}). Various bands such as 3469, 2357, 1686, 1458, 1148, 739 and 422 (cm^{-1}) were noticed. The bands between 400 and 700 cm^{-1} are associated with Fe–O groups (Karpagavinayagam and Vedhi, 2019). The medium band at 739 cm^{-1} and a small band at 422 cm^{-1} confirmed the Fe–O bending vibrations (Aksu Demirezen, Yıldız, Yılmaz, et al., 2019). Also, the band at 1148 cm^{-1} corresponded to the vibration of crystalline Fe–O mode which is the characteristic feature of Fe_2O_3 (Maji et al., 2012). The wide band observed at 3469 denoted O–H stretching (Pugazhendhi et al., 2019), which revealed the phenolic compounds of CPLE (Sebastian et al., 2019). The 1660 cm^{-1} band belonged to the C=C stretching vibration of alkenes (Raut et al., 2014; Vasantharaj et al., 2019b). A sharp band at 2357 cm^{-1} corresponded to the S–N vibrations of L-cysteine present in CPLE (Raja et al., 2015; Varadavenkatesan et al., 2017).

Another sharp band at 1458 cm^{-1} belonged to C–H scissoring and bending of alkane functional groups present in CPLE. Hence, these specific bands endorse the interaction of phyto-compounds of CPLE which showed a significant role in the formation of CP–FONPs. Moreover, their presence provides stabilization to the CP–FONPs (Khalil et al., 2017).

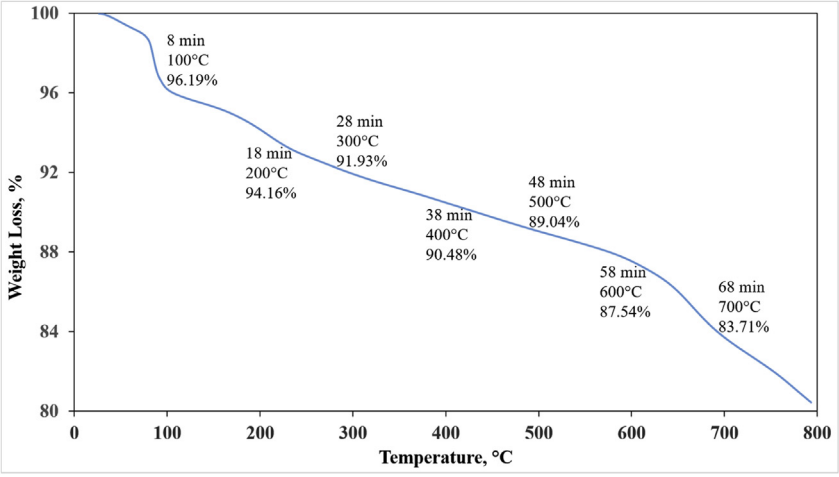

Fig. 7. TGA curve of the CP–FONPs.

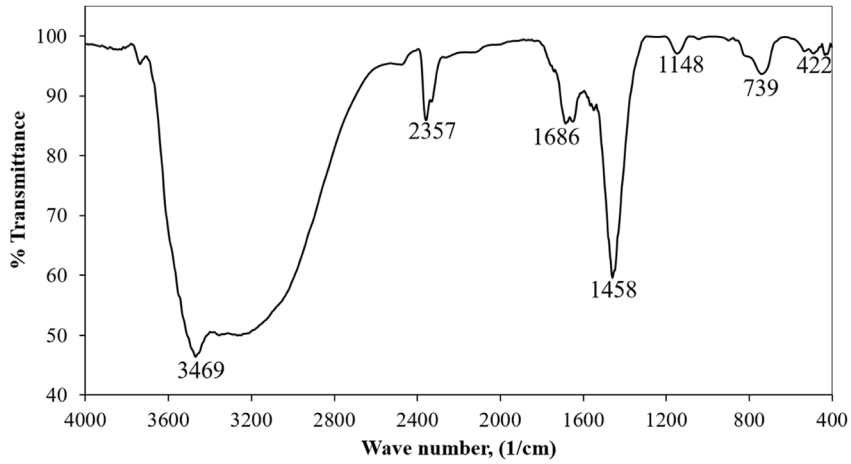

Fig. 8. FTIR spectrum of the CP–FONPs.

3.7. Fenton-like catalytic activity of CP–FONPs for the degradation of MB dye

Fig. 9 demonstrates the decolorization of MB dye by CP–FONPs in the presence of H_2O_2. The bottle A which had MB dye and H_2O_2 did not display any significant reduction in the color while the vial B which contained CP–FONPs along with MB dye and H_2O_2 showed substantial changes in the color intensity. The decline in absorbance at 665 nm with time can be visualized. The degradation starts instantaneously with approximately 50% of the dye being degraded within 5 min reaction time. Almost 90% of dye was degraded within 220 min (Fig. 9: Inset C). It is believed that the rapidness of the degradation process may be due to the +3 oxidation state of the iron present in FONPs which enhances the degradation process (Xue et al., 2009). The final color of the vial B and the attraction of CP–FONPs towards the magnet confirmed the retention of magnetic separation capacity of nanoparticles (Fig. 9: Inset B).

Eqs. (1) and (2) were used to fit the decolorization data and the linear plots are shown in Fig. 10. It is evident from the figure that excellent linearity is obtained for the second order model. The linear correlation coefficient (R^2) values were 0.735 and 0.963 for the first and second order models respectively. Similarly, the degradation rate constants, K_1 and K_2 were 0.0395 min^{-1} and 0.0987 L/mg min respectively (Table 2). Therefore, the second order kinetics best fits the decolorization process. Similar kind of conclusions was obtained for the MB dye degradation by green-synthesized iron nanoparticles in the presence of H_2O_2 (Shahwan et al., 2011).

For the decolorization of MB dye, the generation of highly reactive hydroxyl radicals (HO•) is important. In the Fenton-like process, these are generated in a series of reactions as given by Eqn. (3–5)

$$Fe^{3+} + H_2O_2 \rightarrow Fe^{3+}(H_2O_2) \quad (3)$$

$$Fe^{3+}(H_2O_2) \rightarrow Fe^{2+} + H^+ + HO_2\bullet \quad (4)$$

$$Fe^{2+} + H_2O_2 \rightarrow Fe^{3+} + OH^- + HO\bullet \quad (5)$$

Briefly, in the first reaction, the ferric ion (Fe^{3+}) from the CP–FONPs forms an intermediate, $Fe^{3+}(H_2O_2)$ by the adsorption of H_2O_2 on its surface (Eqn. (3)). This intermediate disassociates to form Fe^{2+}, H^+ and hydroperoxyl radical ($HO_2\bullet$) in the second reaction (Eqn. (4)). In the end, this Fe^{2+} is oxidized to form Fe^{3+}, OH^- and (HO•) radicals (Eqn. (5)). The (HO•) were generated continuously because of the strong oxidation capacity of H_2O_2 (Li et al., 2019). Thus, the generated (HO•) acts on MB dye to give non-toxic products such as CO_2 and H_2O (Eqn. (6)).

$$\text{MB dye} + HO\bullet \rightarrow nCO_2 + nH_2O \quad (6)$$

A similar type of mechanism was reported by many researchers for the degradation of dyes by Fenton-like catalysts such as commercially available iron (II, III) oxide nanoparticles (Xue et al., 2009), green

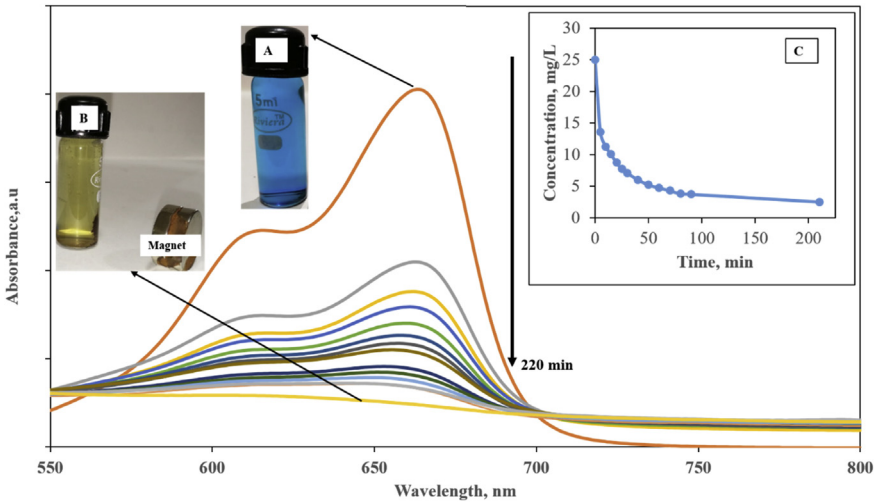

Fig. 9. Degradation of MB dye with time in the presence of CP–FONPs and H_2O_2 (Inset: (A) Initial color, (B) Final color, (C) Plot of MB dye concentration vs. time. (For interpretation of the references to color in this figure legend, the reader is referred to the Web version of this article.)

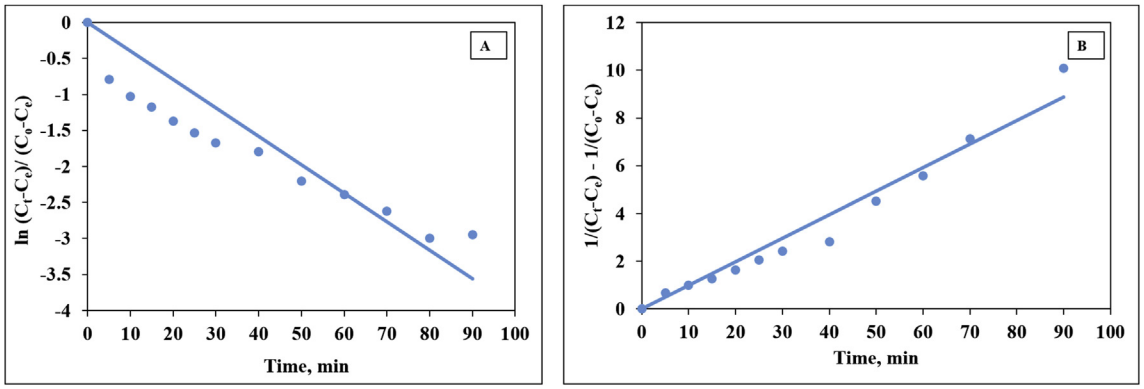

Fig. 10. Linear plots of decolorization of MB dye (A) first order, (B) Second order.

Table 2
Kinetics constants' values of linear regression models for MB dye degradation.

Reaction Type	First order		Second order	
	K_1 (min^{-1})	R^2	K_2 (L/mg min)	R^2
Fenton-like degradation	0.0395	0.735	0.0987	0.963
$NaBH_4$ mediated degradation	0.0856	0.971	0.0131	0.782

-synthesized iron nanoparticles (Garole et al., 2018) (Groiss et al., 2017).

3.8. Degradation of MB dye with CP–FONPs and $NaBH_4$

It is known that the decolorization of MB dye by $NaBH_4$ is a slow process (Selvaraj, Raja; Yadav, P. Manjunath, 2019). In general, nanocatalysts can make the reaction kinetically possible by decreasing the time (Naseem et al., 2019). Thus, to enhance the degradation process and verify the catalytic activity of CP–FONPs, it was added to the reaction mixture, and UV–visible spectra were used to monitor the progress of degradation.

The rapid decreasing trend in the absorbance spectra and the characteristic MB dye peak at 665 nm can be visualized from Fig. 11. The original color of the MB dye (Fig. 11: Inset A) was almost completely lost (Fig. 11: Inset B) within 27 min of reaction in the presence of CP–FONPs. The magnetic attraction of the reacted CP–FONPs can also be witnessed here. The degradation process depicted 92% removal of the dye (Fig. 11: Inset C). The results are comparable with the existing report (Cheera et al., 2016), in which it took 30 min to remove 96% of MB dye using iron oxide nanoparticles, green-synthesized using *Ridge gourd* peel extract.

It is quoted that the decrease in the absorbance value at 665 nm is because of the breaking down of double bond in the chromophore of MB dye by hydrogen which was liberated from $NaBH_4$(Cheera et al., 2016)(Edison et al., 2016). The mechanism of dye degradation can be explained by a process known as "electron relay process" (Selvaraj, Raja; Yadav, P. Manjunath, 2019), in which BH_4^- ions transfer electrons to CP–FONPs and creates a negatively charged environment. Later, the electrons degrade the MB dye to harmless products (Fig. 12). Very recently, a similar type of mechanism has been reported for MB dye degradation by silver nanoparticles impregnated core-shell composite microgels (Naseem et al., 2019). In this article, they stated that BH_4^- ions are nucleophilic whereas MB dye molecules are electrophilic. Therefore, in the degradation process, MB dye receives electrons from BH_4^- through CP–FONPs which play a role of the electron-conveyor belt between BH_4^- and dye molecules.

Furthermore, the catalytic activity of the CP–FONPs may be due to the reduction potential of Fe^{3+} (+0.77 V) (Zakharov et al., 2011) which is higher than that of MB dye (0.011 V) (Liu et al., 2013). Hence, the Fe^{3+} ions can rapidly reduce the MB dye. The mechanism based on reduction potential has been well explained for the removal of Cr^{6+} using the iron-based nanoparticles from the extracts of *Nephrolepis auriculata* (Yi et al., 2019).

Similar to the Fenton-like process, the kinetic data of this degradation process were also fitted to Eqs. (1) and (2). However, it was found that the first order model (Fig. 13: Inset A) fitted better to the kinetic data with K_1 of 0.0856 min^{-1} and R^2 of 0.971 (Table 2). On the other hand, the second order model (Fig. 12: Inset B) yielded a K_2 of

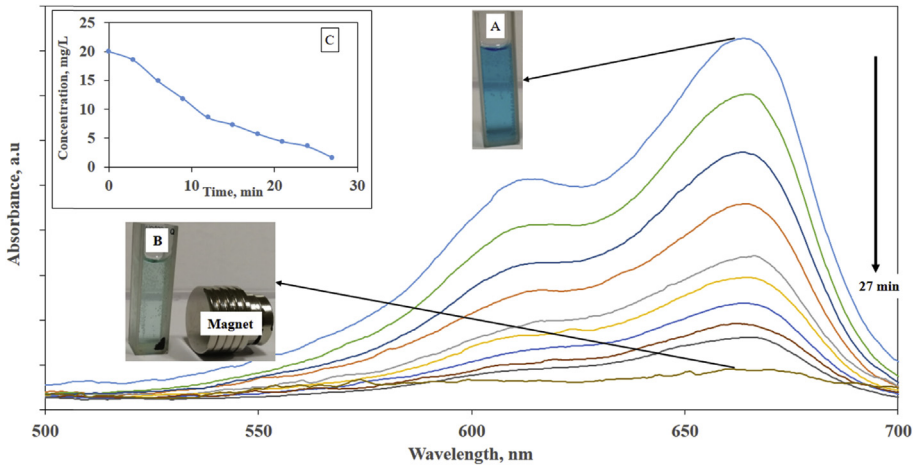

Fig. 11. Catalytic degradation of MB dye with CP–FONPs and $NaBH_4$ (Inset: (A) Initial color, (B) Final color, (C) Plot of MB dye concentration vs. time. (For interpretation of the references to color in this figure legend, the reader is referred to the Web version of this article.)

Fig. 12. Mechanism of degradation of MB dye in the presence of CP–FONPs and $NaBH_4$.

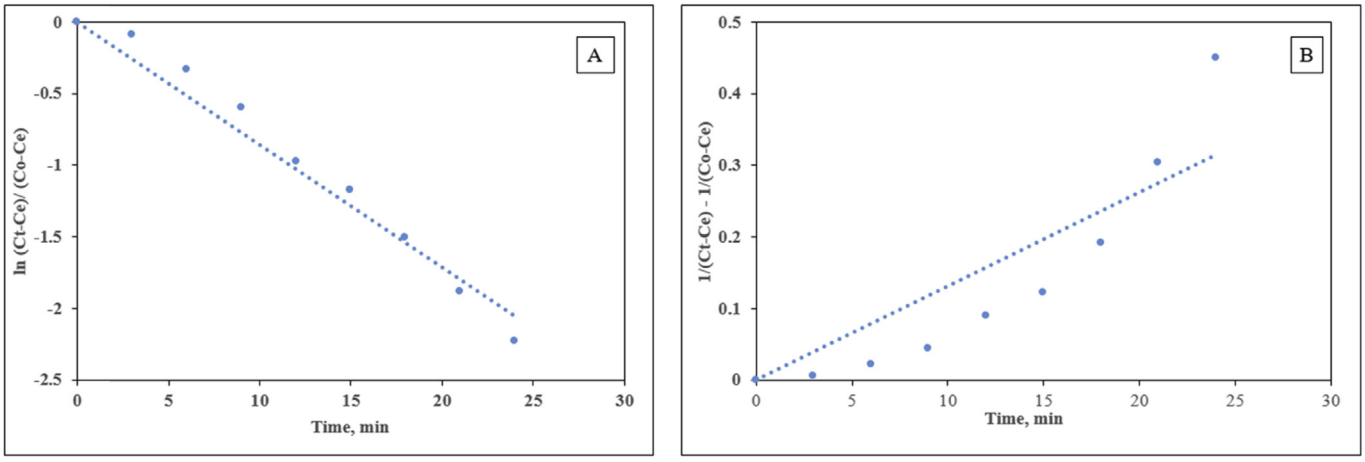

Fig. 13. Linear plots of decolorization of MB dye with CP–FONPs and $NaBH_4$ (A) first order, (B) Second order.

0.0131 L/mg min and R^2 of 0.782. It should be noted here that the higher the value of the rate constant, the degradation process will be faster (Shahwan et al., 2011). The rapid degradation observed in this study may be due to the large surface area of CP–FONPs which could have provided many catalytic sites for the reaction.

4. Conclusions

In the present study, the leaf extract of *P.pterocarpum* was utilized as a reducing agent to synthesize FONPs from $FeSO_4$ successfully. This is the first report on the synthesis of FONPs using *P.pterocarpum* leaf extract. The process did not employ either any toxic chemical or energy-intensive step. Hence, the process is simple, rapid, cheap and environmentally benign. The synthesized FONPs were well-characterized by various methods. XRD data ascertained the presence of γ and α phase of Fe_2O_3. The higher surface area was obtained than commercial FONPs, and mesoporous nature was ascertained from the BET results. FTIR results showed specific bands for Fe–O. The synthesized FONPs exhibited excellent catalytic ability to degrade MB dye by Fenton-like process and $NaBH_4$-mediated degradation process. The mesoporous and high surface area of FONPs synthesized in this method hastened the process of dye degradation, and this outcome paves the way for remediation of harmful dyes from wastewater in the field of nanoremediation.

Declarations of interests

None.

Acknowledgment

All the authors would like to thank the Department of Civil engineering and Department of Chemical engineering, Manipal Institute of Technology (MIT), Manipal Academy of Higher Education (MAHE) for providing all the facilities to perform the research work. In addition, the authors thank DST PURSE Laboratory, Mangalore University, Mangalagangotri for providing the FE-SEM facilities and Sophisticated Test & Instrumentation Centre, Cochin University of Science and Technology, Cochin, Kerala for EDS facilities.

References

Ahmmad, Bashir, Leonard, Kwati, Islam, Md Shariful, Kurawaki, Junichi, Muruganandham, Manickavachagam, Ohkubo, Takahiro, Kuroda, Yasushige, 2013. Green synthesis of mesoporous hematite (α-Fe2O3) nanoparticles and their photocatalytic activity. Adv. Powder Technol. 24 (1), 160–167.

Aksu Demirezen, Derya, Yıldız, Yalçın Şevki, Yılmaz, Dilek Demirezen, 2019a. Amoxicillin degradation using green synthesized iron oxide nanoparticles: kinetics and mechanism analysis. Environ. Nanotechnol. Monitor. Manage. 11, 100219.

Aksu Demirezen, Derya, Yıldız, Yalçın Şevki, Yılmaz, Şeyda, Yılmaz, Dilek Demirezen, 2019b. Green synthesis and characterization of iron oxide nanoparticles using Ficus carica (common fig) dried fruit extract. J. Biosci. Bioeng. 127 (2), 241–245.

Amstad, Esther, Marcus, Textor, Reimhult, Erik, 2011. Stabilization and functionalization of iron oxide nanoparticles for biomedical applications. Nanoscale 3 (7), 2819–2843.

Asoufi, Hassan M., Al-Antary, Tawfiq M., Awwad, Akl M., 2018. "Green route for synthesis hematite (α-Fe2O3) nanoparticles: toxicity effect on the green peach aphid, Myzus persicae (sulzer)." *environmental nanotechnology*. Monitor. Manage. 9, 107–111.

Balamurugan, Matheswaran, Saravanan, Shanmugam, Soga, Tetsuo, 2014. Synthesis of iron oxide nanoparticles by using *Eucalyptus globulus* plant extract. E-J Surface. Sci. Nanotechnol. 12, 363–367.

Basavegowda, Nagaraj, Mishra, Kanchan, Lee, Yong Rok, 2017. Synthesis, characterization, and catalytic applications of hematite (α-Fe2O3) nanoparticles as reusable nanocatalyst. Adv. Nat. Sci. Nanosci. Nanotechnol. 8 (2), 25017.

Bishnoi, Shahana, Kumar, Aarti, Selvaraj, Raja, 2018. Facile synthesis of magnetic iron oxide nanoparticles using inedible Cynometra ramiflora fruit extract waste and their photocatalytic degradation of methylene blue dye. Mater. Res. Bull. 97, 121–127.

Carvalho, Samira S.F., Carvalho, Nakédia M.F., 2017. Dye degradation by green heterogeneous Fenton catalysts prepared in presence of Camellia sinensis. J. Environ. Manag. 187, 82–88.

Cheera, Prasad, Karlapudi, Sreenivasulu, Sellola, Gangadhara, Ponneri, Venkateswarlu, 2016. A facile green synthesis of spherical Fe3O4 magnetic nanoparticles and their effect on degradation of methylene blue in aqueous solution. J. Mol. Liq. 221, 993–998.

Dash, Asiman, Ahmed, Mohammed Tameem, Selvaraj, Raja, 2019. Mesoporous magnetite nanoparticles synthesis using the Peltophorum pterocarpum pod extract, their antibacterial efficacy against pathogens and ability to remove a pollutant dye. J. Mol. Struct. 1178, 268–273.

Edison, Thomas Nesakumar Jebakumar Immanuel, Lee, Yong Rok, Sethuraman, Mathur Gopalakrishnan, 2016. Green synthesis of silver nanoparticles using Terminalia cuneata and its catalytic action in reduction of direct yellow-12 dye. Spectrochim. Acta A Mol. Biomol. Spectrosc. 161, 122–129.

Farshchi, Helale Kaboli, Azizi, Majid, Jaafari, Mahmoud Reza, Nemati, Seyyd Hossien,

Fotovat, Amir, 2018. Green synthesis of iron nanoparticles by rosemary extract and cytotoxicity effect evaluation on cancer cell lines. Biocatalysis. Agri Biotechnol. 16, 54–62.
Fathima, John Bani, Pugazhendhi, Arivalagan, Oves, Mohammad, Venis, Rose, 2018. Synthesis of eco-friendly copper nanoparticles for augmentation of catalytic degradation of organic dyes. J. Mol. Liq. 260, 1–8.
García, Fabiana E., Senn, Alejandro M., Meichtry, Jorge M., Scott, Thomas B., Pullin, Huw, Leyva, Ana G., Halac, Emilia B., Ramos, Cinthia P., Sacanell, Joaquín, Mizrahi, M., Requejo, Félix G., Litter, Marta I., 2019. Iron-based nanoparticles prepared from yerba mate extract. Synthesis, characterization and use on chromium removal. J. Environ. Manag. 235 (December 2018), 1–8.
Garole, V.J., Choudhary, B.C., Tetgure, S.R., Garole, D.J., Borse, A.U., 2018. Detoxification of toxic dyes using biosynthesized iron nanoparticles by photo-fenton processes. Int. J. Environ. Sci. Technol. 15 (8), 1649–1656.
Groiss, Silvia, Selvaraj, Raja, Varadavenkatesan, Thivaharan, Vinayagam, Ramesh, 2017. Structural characterization, antibacterial and catalytic effect of iron oxide nanoparticles synthesised using the leaf extract of Cynometra ramiflora. J. Mol. Struct. 1128, 572–578.
Guo, Sheng, Zhang, Gaoke, Wang, Jiquan, 2014. Photo-fenton degradation of rhodamine B using Fe2O3–kaolin as heterogeneous catalyst: characterization, process optimization and mechanism. J. Colloid Interface Sci. 433, 1–8.
Hoag, George E., Collins, John B., Holcomb, Jennifer L., Hoag, Jessica R., Nadagouda, Mallikarjuna N., Rajender, S. Varma, 2009. "Degradation of bromothymol blue by 'greener' nano-scale zero-valent iron synthesized using tea polyphenols. J. Mater. Chem. 19 (45), 8671.
Huang, Lanlan, Luo, Fang, Chen, Zuliang, Megharaj, Mallavarapu, Naidu, Ravendra, 2015. Green synthesized conditions impacting on the reactivity of Fe {NPs} for the degradation of malachite green. Spectrochim. Acta A Mol. Biomol. Spectrosc. 137, 154–159.
Hussain, Imtiyaz, Singh, N.B., Singh, Ajey, Singh, Himani, Singh, S.C., 2016. Green synthesis of nanoparticles and its potential application. Biotechnol. Lett. 38 (4), 545–560.
Ju-Nam, Yon, Lead, Jamie R., 2008. Manufactured nanoparticles: an overview of their chemistry, interactions and potential environmental implications. Sci. Total Environ. 400 (1), 396–414.
Karpagavinayagam, P., Vedhi, C., 2019. Green synthesis of iron oxide nanoparticles using Avicennia marina flower extract. Vacuum 160, 286–292.
Khalil, Ali Talha, Ovais, Muhammad, Ullah, Ikram, Ali, Muhammad, Khan Shinwari, Zabta, Malik, Maaza, 2017. Biosynthesis of iron oxide (Fe2O3) nanoparticles via aqueous extracts of Sageretia thea (osbeck.) and their pharmacognostic properties. Green Chem. Lett. Rev. 10 (4), 186–201.
Kharissova, Oxana V., Dias, H. V. Rasika, Kharisov, Boris I., Pérez, Betsabee Olvera, Victor, M., Pérez, Jiménez, 2013. The greener synthesis of nanoparticles. Trends Biotechnol. 31 (4), 240–248.
Khatami, Mehrdad, Alijani, Hajar Q., Fakheri, Baratali, Mobasseri, Mohammad M., Heydarpour, Masoomeh, Farahani, Zeinab K., Khan, Arif Ullah, 2019. Super-paramagnetic iron oxide nanoparticles (SPIONs): greener synthesis using stevia plant and evaluation of its antioxidant properties. J. Clean. Prod. 208, 1171–1177.
Kumar, Brajesh, Smita, Kumari, Cumbal, Luis, Debut, Alexis, Galeas, Salome, Guerrero, Victor H., 2016. Phytosynthesis and photocatalytic activity of magnetite (Fe3O4) nanoparticles using the andean blackberry leaf. Mater. Chem. Phys. 179, 310–315.
Li, Huosheng, Li, Xiuwan, Long, Jianyou, Li, Keke, Chen, Yongheng, Jiang, Jiahao, Chen, Xiaoxuan, Zhang, Ping, 2019. Oxidation and removal of thallium and organics from wastewater using a zero-valent-iron-based fenton-like technique. J. Clean. Prod. 221, 89–97.
Litvin, V.A., Minaev, B.F., 2013. Spectroscopy study of silver nanoparticles fabrication using synthetic humic substances and their antimicrobial activity. Spectrochim. Acta A Mol. Biomol. Spectrosc. 108, 115–122.
Liu, Xian-Wei, Sun, Xue-Fei, Chen, Jie-Jie, Huang, Yu-Xi, Xie, Jia-Fang, Li, Wen-Wei, Sheng, Guo-Ping, Zhang, Yuan-Yuan, Zhao, Feng, Lu, Rui, Han-Qing, Yu, 2013. Phenothiazine derivative-accelerated microbial extracellular electron transfer in bioelectrochemical system. Sci. Rep. 3, 1616.
Maji, Swarup Kumar, Mukherjee, Nillohit, Mondal, Anup, Adhikary, Bibhutosh, 2012. Synthesis, characterization and photocatalytic activity of α-Fe2O3 nanoparticles. Polyhedron 33 (1), 145–149.
Makarov, Valentin V., Makarova, Svetlana S., Love, Andrew J., Sinitsyna, Olga V., Dudnik, Anna O., Yaminsky, Igor V., Taliansky, Michael E., Kalinina, Natalia O., 2014. Biosynthesis of stable iron oxide nanoparticles in aqueous extracts of hordeum vulgare and rumex acetosa plants. Langmuir 30 (20), 5982–5988.
Mishra, Maneesha, Chun, Doo-Man, 2015. α-Fe2O3 as a photocatalytic material: a review. Appl. Catal. Gen. 498, 126–141.
Mukherjee, Debarati, Ghosh, Sourja, Majumdar, Swachchha, Annapurna, K., 2016. Green synthesis of α-Fe2O3 nanoparticles for arsenic(V) remediation with a novel aspect for sludge management. J. Environ. Chem Eng. 4 (1), 639–650.
Nandhini, N.T., Rajeshkumar, S., Mythili, S., 2019. The possible mechanism of eco-friendly synthesized nanoparticles on hazardous dyes degradation. Biocatalysis. Agri Biotechnol. 19, 101138.
Narayanan, Kannan Badri, Han, Sung Soo, 2016. One-pot green synthesis of hematite (α-Fe2O3) nanoparticles by ultrasonic irradiation and their in vitro cytotoxicity on human keratinocytes CRL-2310. J. Clust. Sci. 27 (5), 1763–1775.
Naseem, Khalida, Begum, Robina, Wu, Weitai, Ahmad, Irfan, Abdullah, G., Al-Sehemi, Farooqi, Zahoor H., 2019. Catalytic reduction of toxic dyes in the presence of silver nanoparticles impregnated core-shell composite microgels. J. Clean. Prod. 211, 855–864.
Naz, Sania, Islam, Mohammad, Tabassum, Saira, Fernandes, Nelson Freitas, Esperanza, J., de Blanco, Carcache, Zia, Muhammad, 2019. Green synthesis of hematite (α-Fe2O3) nanoparticles using Rhus punjabensis extract and their biomedical prospect in pathogenic diseases and cancer. J. Mol. Struct. 1185, 1–7.
Njagi, Eric C., Huang, Hui, Stafford, Lisa, Genuino, Homer, Galindo, Hugo M., Collins, John B., Hoag, George E., Suib, Steven L., 2011. Biosynthesis of iron and silver nanoparticles at room temperature using aqueous sorghum bran extracts. Langmuir 27 (1), 264–271.
Pai, Shraddha, Sridevi, H., Varadavenkatesan, Thivaharan, Ramesh, Vinayagam, Raja Selvaraj, 2019. Photocatalytic zinc oxide nanoparticles synthesis using Peltophorum pterocarpum leaf extract and their characterization. Optik 185, 248–255.
Peralta-Videa, Jose, R., Huang, Yuxiong, Parsons, Jason G., Zhao, Lijuan, Lopez-Moreno, Laura, Hernandez-Viezcas, Jose A., Gardea-Torresdey, Jorge L., 2016. Plant-based green synthesis of metallic nanoparticles: scientific curiosity or a realistic alternative to chemical synthesis? Nanotechnol. Environ. Eng. 1 (1), 4.
Pugazhendhi, Arivalagan, Prabhu, Raju, Muruganantham, Kavitha, Shanmuganathan, Rajasree, Natarajan, Suganthy, 2019. Anticancer, antimicrobial and photocatalytic activities of green synthesized magnesium oxide nanoparticles (MgONPs) using aqueous extract of sargassum wightii. J. Photochem. Photobiol. B Biol. 190, 86–97.
Raghunath, Azhwar, Perumal, Ekambaram, 2017. Metal oxide nanoparticles as antimicrobial agents: a promise for the future. Int. J. Antimicrob. Agents 49 (2), 137–152.
Raja, Selvaraj, Ramesh, Vinayagam, Thivaharan, Varadavenkatesan, 2015. "Antibacterial and anticoagulant activity of silver nanoparticles synthesised from a novel source-–pods of Peltophorum pterocarpum. J. Ind. Eng. Chem. 29, 257–264.
Raut, Rajesh Warluji, Mendhulkar, Vijay Damodhar, Balaso Kashid, Sahebrao, 2014. Photosensitized synthesis of silver nanoparticles using withania somnifera leaf powder and silver nitrate. J. Photochem. Photobiol. B Biol. 132, 45–55.
Ruíz-Baltazar, Álvaro de Jesús, Reyes-López, Simón Yobanny, de Lourdes Mondragón-Sánchez, María, Robles-Cortés, Anel Ivonne, Pérez, Ramiro, 2019. Eco-friendly synthesis of Fe3O4 nanoparticles: evaluation of their catalytic activity in methylene blue degradation by kinetic adsorption models. Results in Physics 12, 989–995.
Sahoo, S.K., Agarwal, K., Singh, A.K., Polke, B.G., Raha, K.C., 2010. Characterization of $γ$-and $α$-Fe 2 O 3 nano powders synthesized by emulsion precipitation-calcination route and rheological behaviour of $α$-Fe 2 O 3. Int. J. Eng. Sci. Technol. 2 (8).
Saratale, Rijuta Ganesh, Ghodake, Gajanan S., Shinde, Surendra K., Cho, Si-Kyung, Saratale, Ganesh Dattatraya, Pugazhendhi, Arivalagan, Bharagava, Ram Naresh, 2018. Photocatalytic activity of CuO/Cu(OH)2 nanostructures in the degradation of reactive green 19A and textile effluent, phytotoxicity studies and their biogenic properties (antibacterial and anticancer). J. Environ. Manag. 223, 1086–1097.
Sathiyavimal, Selvam, Vasantharaj, Seerangaraj, Bharathi, Devaraj, Saravanan, Mythili, Manikandan, Elayaperumal, Kumar, Smita S., Pugazhendhi, Arivalagan, 2018. Biogenesis of copper oxide nanoparticles (CuONPs) using Sida acuta and their incorporation over cotton fabrics to prevent the pathogenicity of gram negative and gram positive bacteria. J. Photochem. Photobiol. B Biol. 188, 126–134.
Schröfel, Adam, Kratošová, Gabriela, Šafařík, Ivo, Šafaříková, Mirka, Raška, Ivan, Leslie, M., Shor, 2014. "Applications of biosynthesized metallic nanoparticles – a review. Acta Biomater. 10 (10), 4023–4042.
Sebastian, Abin, Nangia, Ashwini, V Prasad, M.N., 2019. Cadmium and sodium adsorption properties of magnetite nanoparticles synthesized from hevea brasiliensis muell. Arg. Bark: relevance in amelioration of metal stress in rice. J. Hazard Mater. 371, 261–272.
Selvaraj, Raja, Yadav, P., Manjunath, H., 2019. Antibacterial and dye degradation potential of zero-valent silver nanoparticles synthesised using the leaf extract of spondias dulcis. IET Nanobiotechnol. 13 (1), 84–89 (5).
Shahwan, T., Abu Sirriah, S., Nairat, M., Boyacı, E., Eroğlu, A.E., Scott, T.B., Hallam, K.R., 2011. Green synthesis of iron nanoparticles and their application as a fenton-like catalyst for the degradation of aqueous cationic and anionic dyes. Chem. Eng. J. 172 (1), 258–266.
Sirdeshpande, Karthikey Devadatta, Sridhar, Anushka, Cholkar, Kedar Mohan, Selvaraj, Raja, 2018. Structural characterization of mesoporous magnetite nanoparticles synthesized using the leaf extract of calliandra haematocephala and their photocatalytic degradation of malachite green dye. Appl. Nanosci. 8 (4), 675–683.
Sneha, Murugesan, Sundaram, Nachiappan Meenakshi, 2015. Preparation and characterization of an iron oxide-hydroxyapatite nanocomposite for potential bone cancer therapy. Int. J. Nanomed. 10 (Suppl. 1), 99–106.
Thivaharan, Varadavenkatesan, Ramesh, Vinayagam, Selvaraj, Raja, 2018. Green synthesis of silver nanoparticles for biomedical and environmental applications. Green Metal Nanoparticles 287–439.
Varadavenkatesan, T., Selvaraj, R., Vinayagam, R., 2019. Dye degradation and antibacterial activity of green synthesized silver nanoparticles using Ipomoea digitata linn. Flower extract. Int. J. Environ. Sci. Technol. 16 (5), 2395–2404.
Varadavenkatesan, Thivaharan, Ramesh, Vinayagam, Selvaraj, Raja, 2017. Structural characterization of silver nanoparticles phyto-mediated by a plant waste, seed hull of vigna mungo and their biological applications. J. Mol. Struct. 1147, 629–635.
Vasantharaj, S., Sathiyavimal, S., Saravanan, M., Senthilkumar, P., Gnanasekaran, K., Shanmugavel, M., Manikandan, E., Pugazhendhi, A., 2019a. Synthesis of ecofriendly copper oxide nanoparticles for fabrication over textile fabrics: characterization of antibacterial activity and dye degradation potential. J. Photochem. Photobiol. B Biol. 191, 143–149.
Vasantharaj, S., Sathiyavimal, S., Senthilkumar, P., LewisOscar, F., Pugazhendhi, A., 2019b. Biosynthesis of iron oxide nanoparticles using leaf extract of Ruellia tuberosa: antimicrobial properties and their applications in photocatalytic degradation. J. Photochem. Photobiol. B Biol. 192, 74–82.
Vinayagam, Ramesh, Varadavenkatesan, Thivaharan, Selvaraj, Raja, 2017. Evaluation of the anticoagulant and catalytic activities of the bridelia retusa fruit extract-functionalized silver nanoparticles. J. Clust. Sci. 28 (5), 2919–2932.
Vinayagam, Ramesh, Varadavenkatesan, Thivaharan, Selvaraj, Raja, 2018. Green synthesis, structural characterization, and catalytic activity of silver nanoparticles

stabilized with bridelia retusa leaf extract. Green Process. Synth. 7 (1), 30–37.
Wang, Nannan, Tong, Zheng, Zhang, Guangshan, Wang, Peng, 2016. A review on fenton-like processes for organic wastewater treatment. J. Environ. Chem Eng. 4 (1), 762–787.
Weng, Xiulan, Huang, Lanlan, Chen, Zuliang, Megharaj, Mallavarapu, Naidu, Ravendra, 2013. Synthesis of iron-based nanoparticles by green tea extract and their degradation of malachite. Ind. Crops Prod. 51, 342–347.
Xue, Xiaofei, Hanna, Khalil, Deng, Nansheng, 2009. Fenton-like oxidation of rhodamine B in the presence of two types of iron (II, III) oxide. J. Hazard Mater. 166 (1), 407–414.
Yew, Yen Pin, Shameli, Kamyar, Miyake, Mikio, Kuwano, Noriyuki, Bt Ahmad Khairudin, Nurul Bahiyah, Bt Mohamad, Shaza Eva, Lee, Kar Xin, 2016. Green synthesis of magnetite (Fe3O4) nanoparticles using seaweed (kappaphycus alvarezii) extract. Nanoscale Res. Lett. 11 (1), 276.
Yi, Yunqiang, Tu, Guoquan, Pokeung Eric Tsang, Xiao, Shihua, Fang, Zhanqiang, 2019. Green synthesis of iron-based nanoparticles from extracts of Nephrolepis auriculata and applications for Cr(VI) removal. Mater. Lett. 234, 388–391.
Yu, Wan-Jing, Hou, Peng-Xiang, Zhang, Li-Li, Li, Feng, Chang, Liu, Cheng, Hui-Ming, 2010. Preparation and electrochemical property of Fe2O3 nanoparticles-filled carbon nanotubes. Chem. Commun. 46 (45), 8576–8578.
Zakharov, I.I., Kudjukov, K. Yu, V Bondar, V., Tyupalo, N.F., Minaev, B.F., 2011. "DFT-Based thermodynamics of Fenton reactions rejects the 'pure' aquacomplex models. Computate. Theory. Chem. 964 (1), 94–99.
Zha, Shuangxing, Cheng, Ying, Gao, Ying, Chen, Zuliang, Megharaj, Mallavarapu, Naidu, Ravendra, 2014. Nanoscale zero-valent iron as a catalyst for heterogeneous Fenton oxidation of amoxicillin. Chem. Eng. J. 255, 141–148.
Zhang, Guo-Ying, Yan, Feng, Xu, Yan-Yan, Gao, Dong-Zhao, Sun, Ya-Qiu, 2012. Controlled synthesis of mesoporous α-Fe2O3 nanorods and visible light photocatalytic property. Mater. Res. Bull. 47 (3), 625–630.